

## Journal Pre-proof

Polynomial chaos expansion for uncertainty propagation analysis in numerical homogenisation of 2D/3D periodic composite microstructures

J.C. García-Merino, C. Calvo-Jurado, E. García-Macías



PII: S0263-8223(22)00861-3

DOI: <https://doi.org/10.1016/j.compstruct.2022.116130>

Reference: COST 116130

To appear in: *Composite Structures*

Received date: 24 May 2022

Revised date: 1 August 2022

Accepted date: 13 August 2022

Please cite this article as: J.C. García-Merino, C. Calvo-Jurado and E. García-Macías, Polynomial chaos expansion for uncertainty propagation analysis in numerical homogenisation of 2D/3D periodic composite microstructures. *Composite Structures* (2022), doi: <https://doi.org/10.1016/j.compstruct.2022.116130>.

This is a PDF file of an article that has undergone enhancements after acceptance, such as the addition of a cover page and metadata, and formatting for readability, but it is not yet the definitive version of record. This version will undergo additional copyediting, typesetting and review before it is published in its final form, but we are providing this version to give early visibility of the article. Please note that, during the production process, errors may be discovered which could affect the content, and all legal disclaimers that apply to the journal pertain.

© 2022 Elsevier Ltd. All rights reserved.

# Polynomial chaos expansion for uncertainty propagation analysis in numerical homogenisation of 2D/3D periodic composite microstructures

J.C. García-Merino<sup>1</sup>, C. Calvo-Jurado<sup>1</sup>, E. García-Macías<sup>2</sup>

<sup>1</sup>Department of Mathematics, School of Technology, 10003, Cáceres, (Spain), <sup>2</sup>Department of Structural Mechanics and Hydraulic Engineering, Campus Universitario de Fuentenueva (Edificio Politécnico), 18071, Granada (Spain)

---

## Abstract

This paper proposes the use of adaptive polynomial chaos expansion (PCE) for uncertainty propagation analysis of the numerical homogenisation of polymer composites doped with random dispersions of spherical inclusions. The developed PCE acts as a surrogate model bypassing the computationally intense numerical homogenisation of the elastic properties of 2D/3D representative volume elements (RVEs) loaded with moderate to high filler contents. Numerical results and discussion are presented to assess the accuracy and computational efficiency of 2D and 3D homogenization meta-models. The ability of the developed approaches to perform uncertainty propagation analyses with minimum computational effort represents the main contribution of this work, which holds vast potential for the stochastic design of macroscopic composite structural elements.

*Keywords:* Composites, Homogenisation, Linear elasticity, Polynomial chaos expansion, Surrogate modelling, Uncertainty propagation

*2000 MSC:* 35Q74, 35Q82, 74Q15, 74B99.

---

## 1. Introduction

The development of composite materials constitutes an issue of great interest since the 1960s due to their numerous applications in Science and Engineering [1]. Predicting the effective mechanical properties of composite materials is often a challenging problem, involving complex microstructures with multi-scale and highly heterogeneous properties. To address this issue, a large variety of different homogenisation methods have been proposed in the literature [2]. These range from analytical mean-field homogenisation approaches [3, 4] to numerical techniques using finite element modelling (FEM) [5], boundary elements methods (BEM) [6, 7, 8], atomistic-based continuum mechanics [9], molecular dynamics simulations (MDS) [10], Virtual FEM (VEM) [11, 12, 13] and Fast Fourier Transform techniques [14], just to mention a few. Numerical methods are particularly popular owing to their ability to represent the exact geometry of complex microstructures [15], keeping minimal the number of assumptions and simplifications of the underlying microstructure [5]. Nonetheless, these approaches suffer from large computational demands due to the elevated mesh densities usually required to discretize RVEs. This represents a major limitation in various applications where numerous model evaluations are required, namely optimization, inverse calibration, uncertainty propagation or reliability analyses.

The simplest numerical homogenization approach consists in the use of periodic unit cells [16] containing a canonical arrangement of particles which are assumed to replicate periodically throughout the composite material. However, most composite materials present a certain degree of randomness in the dispersion of the doping

fillers. The problem of the determination of the effective behavior of random composite materials has been extensively treated in the literature. Theoretical approaches span from classical bounds for two-phase composites [17] to analytical [18, 19] or numerical [20, 21] homogenisation techniques. Moreover, considerable research efforts have been exerted toward the definition of accurate RVEs for heterogeneous materials through the analysis of convergence rates in computational homogenization approaches (see e.g. [22, 23]). In general, algorithms for the generation of random microstructures can be firstly classified according to the dimensions of the RVE, namely 2D or 3D. Two-dimensional models represent a cost-efficient approach particularly well-suited for composite materials with uni-axial symmetry such as fully aligned fiber-reinforced composites [24]. Nonetheless, many composite materials present complex microstructures that can hardly be represented by 2D models, being imperative to implement more computationally intense 3D RVEs [25]. In this regard, several works in the literature have reported about the applicability and limitations of two- and three-dimensional RVEs. It is worth noting the work by Nil and co-authors [26] who presented a comparison between 3D and 2D homogenised RVEs of meso-scale concrete. Their results showed that the effective diffusivity of the 3D model is about 1.4 times that of the 2D model. The effects of aggregate/void areas on the homogenised elastic and tensile fracture behaviours of concrete using 2D and 3D RVEs was also investigated by Hua *et al.* [27]. In that work, a 3D model was constructed from 2D images by a bottom-up stacking algorithm, therefore the resultant 3D model is strongly correlated to the 2D. In reference [28], the stresses of 2D and 3D RVEs of porous polymer material were investigated and compared. Those authors concluded that if 2D model reliably represents the 3D geometry, then the deformation behaviour can be analysed using the 2D RVE as the difference between stresses red obtained by the 2D and 3D RVEs do not exceed 10%. On the other hand, algorithms are also often classified according to the procedure used to define the filler distribution, namely dynamic (i), constructive (ii), non-sequential (iii), and discrete element simulations (iv). Dynamic algorithms are often considerably time consuming, since they need to update the position and interactions of the particles. Popular dynamic approaches are the movement and mechanical contraction or growth algorithms [29, 30]. While easily implementable, the convergence rate of these algorithms for moderate to large filler contents is very limited, being hard to achieve filler contents above 30%. On the other hand, constructive algorithms have lower computational burden since the position of the particles are sequentially defined. Among this class of algorithms, one of the most intuitive is the Random Sequential Algorithm [31] (RSA), in which the location of any particle is randomly defined and accepted if it does not overlap with any of the previously located ones. Nonetheless, one of the major drawbacks of RSA regards the limited filler volume fractions that can be achieved, which usually limits to about 30% in 3D geometries [32]. Alternatively, constructive algorithms using dropping and rolling rules allows to evaluate the elastic properties of highly loaded composite materials. These algorithms simulate the process of spheres dropping into a dimension-specified cell when subjected to a gravitational field [33], allowing one to achieve high filler concentrations with limited computational costs. Non-sequential algorithms simulate a very dense distribution of large overlapping spheres that can move to reduce the degree of overlapping [34]. Finally, discrete element methods simulate filler packing as a dynamic process where inter-particle forces are explicitly accounted for [35].

While numerical homogenization methods provide a faithful representation of microstructural composites, their inherent computational demands limit their applicability in resource-intensive applications such as optimization or probabilistic design. In this light, recent developments in the realm of surrogate modelling have opened

vast new possibilities to overcome such limitations. Roughly speaking, meta-models or surrogate models represent computationally lighter representations of parent models [36, 37]. Once constructed, a surrogate model may be considered as a black-box representation of the original model, in many applications with computational costs several orders of magnitude lower. Despite their obvious potential, only a few research works in the literature report about the use of surrogate models for fast homogenisation of composite structures. A noteworthy contribution was done by Dey and co-authors [38], who proposed a fuzzy membership function to identify parameter uncertainties in the characteristics analysis of noise in laminated composites. Peng *et al.* [39] proposed an uncertainty analysis method for composite laminated plates using PCE under insufficient input data related to uncertain design parameters. To that aim, the parameters space was divided according to the observation significance level of the variables. PCE methods are particularly well-suited for uncertainty propagation analysis since the expansion functions are intrinsically defined in stochastic terms [40, 41, 42]. In addition, PCE offers a direct framework for Global Sensitivity Analysis [43], allowing to compute Sobol's indices with the relative importance of the input random variables with no additional function evaluations [43]. Furthermore, PCE methods represent a non-intrusive technique, which results particularly useful when the parent model is defined through commercial software where access to the core scripts is not granted. In this line, Tha *et al.* [36] developed a stochastic multi-scale model for the uncertainty quantification of carbon fiber reinforced composites. In that work, a PCE model was trained using data sets constructed by Monte Carlo simulations of a numerical homogenisation model covering the design space of the parameters and the so called quantities of interest (QoIs), i.e. the corresponding model evaluations on the experimental design (ED).

In light of the discussion above, this work proposes a computationally efficient surrogate model based on adaptive PCE for fast evaluation and uncertainty propagation analysis of the elastic properties of composite materials obtained by 2D/3D numerical homogenization. To minimize the computational cost and maximize the robustness of the meta-model, adaptive sparse expansions are implemented based on the Least Angle Regression (LAR) algorithm [44]. This technique automatically identifies the optimal order of the polynomials in the PCE by a model selection technique for sparse linear models. This work focuses on the elastic properties of epoxy doped with glass fiber spherical inclusions, although the presented approach is general for any composite material. The training datasets are generated using 2D and 3D RVEs discretized by FEM with periodic boundary conditions. The location of the particles are defined using dropping and rolling rules, which allows to obtain filler volume fractions up to 50%. Once constructed, the surrogate models are used to assess the effects of uncertainties in the properties of the micro-constituents on the overall elastic properties of the composite. Finally, numerical results and discussion are presented to appraise the uncertainty propagation effects in 2D and 3D RVEs.

The remainder of this work is organized as follows. Section 2 presents the mathematical formulation of the elastic homogenisation of composite materials, including the theoretical fundamentals of the random packing of particles. Section 3 outlines the theoretical formulation of PCE, and Section 4 presents the proposed surrogate model-based uncertainty propagation analysis of composite materials. Section 5 presents the numerical results and discussion and, finally, Section 6 concludes the paper.

## 2. Statement of the problem

Working in Cartesian coordinates and denoting  $\mathbf{x} = (x, y, z)$ , we restrict our attention in this work to a two-phase composite occupying a domain  $\Omega \subset \mathbb{R}^3$ . Within this domain,  $\Omega_1$  is identified as the inclusion phase or filler (glass particles) embedded into the host phase or matrix (epoxy)  $\Omega_0$ , with respective boundaries  $\Gamma_1$ ,  $\Gamma_0$ , and satisfying  $\Omega = \Omega_1 \cup \Omega_0$ ,  $\Omega_1 \cap \Omega_0 = \emptyset$ . The volume fractions  $\xi_1$  and  $\xi_0$  of the inclusions and matrix phases, respectively, are defined as:

$$\xi_s = \frac{|\Omega_s|}{|\Omega|} = \frac{1}{|\Omega|} \int_{\Omega} \chi_s(\mathbf{x}) d\mathbf{x}, \quad s = 0, 1 \quad \text{subject to} \quad \xi_1 + \xi_0 = 1, \quad (1)$$

where  $|\cdot|$  relates the volume of the constituent phases, and  $\chi_s(\mathbf{x})$  is the characteristic function taking a value of one when  $\mathbf{x} \in \Omega_s$  and zero otherwise. The governing equations of the elastic response of the body to a certain boundary force field  $\mathbf{t}$ , a imposed displacement field at the boundary  $\bar{\mathbf{u}}$ , and a volume force field  $\mathbf{g}$  is given by an elliptic steady-state problem:

$$\begin{cases} -\text{div} [\mathbf{C}(\mathbf{x})\boldsymbol{\varepsilon}(\mathbf{x})] = \mathbf{g} & \text{in } \Omega \\ \mathbf{u}(\mathbf{x}) = \bar{\mathbf{u}} & \text{on } \Gamma_0 \\ \mathbf{C}(\mathbf{x})\boldsymbol{\varepsilon}(\mathbf{x}) \cdot \mathbf{n} = \mathbf{t} & \text{on } \Gamma_1 \end{cases} \quad (2)$$

where  $\mathbf{u}(\mathbf{x})$  is the displacement field,  $\Gamma_0 \cup \Gamma_1 = \Gamma$  with  $\Gamma_0 \cap \Gamma_1 = \emptyset$ , and  $\mathbf{n}$  the outer unit normal to the domain boundary  $\Gamma$ . The strain tensor  $\boldsymbol{\varepsilon}(\mathbf{x})$  is a fourth-order tensor, whose components in Mandel-Voigt notation can be derived from the displacement field  $\mathbf{u}(\mathbf{x})$  as:

$$\varepsilon_{ij} = \frac{1}{2} \left( \frac{\partial u_i}{\partial x_j} + \frac{\partial u_j}{\partial x_i} \right), \quad (3)$$

and it is related to the stress tensor by the generalized Hooke's law  $\boldsymbol{\sigma}(\mathbf{x}) = \mathbf{C}(\mathbf{x})\boldsymbol{\varepsilon}(\mathbf{x})$ . The stiffness tensor  $\mathbf{C}(\mathbf{x})$  of a material point  $\mathbf{x}$  is given by:

$$\mathbf{C}(\mathbf{x}) = \begin{cases} \mathbf{C}^0 & \text{if } \mathbf{x} \in \Omega_0 \\ \mathbf{C}^1 & \text{if } \mathbf{x} \in \Omega_1 \end{cases} \quad (4)$$

with  $\mathbf{C}^1$  and  $\mathbf{C}^0$  the elastic tensors of the filler and the matrix, respectively. Extracting the exact solution of the displacement field from Eq. (2) is a challenging task, and closed-form solutions can only be found for simplified or ideal composite microstructures. Nevertheless, in practical applications, it is usual to characterize the macroscopic effective properties of the composite, represented by a fourth order elastic tensor  $\mathbf{C}^*$  satisfying the homogenised problem of Eq. (2) given by:

$$\begin{cases} -\text{div} [\mathbf{C}^*\boldsymbol{\varepsilon}(\mathbf{x})] = \mathbf{g} & \text{in } \Omega \\ \mathbf{u}(\mathbf{x}) = \bar{\mathbf{u}} & \text{on } \Gamma_0 \\ \mathbf{C}^*\boldsymbol{\varepsilon} \cdot \mathbf{n} = \mathbf{t} & \text{on } \Gamma_1 \end{cases} \quad (5)$$

A variety of techniques have been proposed in the literature to solve the homogenization problem in Eq. (5), being numerical homogenization techniques particularly popular owing to their ability to faithfully represent the microstructure of the composite. These approaches are based on the definition of a RVE containing a sufficient

number of inclusions to statistically represent the composite as a whole. Then, the RVE is subjected to a series of virtual tests by imposing certain boundary conditions on its external faces. The most commonly adopted approaches are Dirichlet (imposed displacements), Neumann (imposed forces), and periodic boundary conditions. In this work, periodic boundary conditions are adopted due to their recognized higher accuracy for low- to medium-scale RVEs [45], thereby geometrical periodicity will be imposed on the RVE. Let us focus in this work on spherical inclusions of radius  $r$ , and cubic (square) RVEs of edge length  $L$ . In order to reach high filler volume fractions, the dropping and rolling rules are considered in this work. This algorithm describes an iterative process where inclusions are sequentially introduced in a RVE under a gravitational field, and rigid contacts and sliding with pre-existing particles define the stacking process [33]. The filler volume fraction is controlled via the inter-particle parameter  $e$  describing the minimal distance between particles. In a 2D context, the algorithm is organized into four main steps as sketched in Fig. 1:

1. Considering gravity along the  $y$ -axis, generate the coordinate centre  $(x, y)$  of a particle, where  $x$  is randomly chosen and  $y$  is located above the top face of the RVE. Then, the particle is moved sequentially with linear trajectory of decreasing  $y$  (Fig. 1 (a)).
2. If the particle contacts the floor of the box, it is assumed that it reaches its final position, and we return to Step 1 (Figs. 1 (a), (d)).
3. Otherwise, rolling rules minimizing the sphere gravity potential are applied. This means that the generated sphere rolls down over its contacting particle/particles until it reaches a stable position (with the minimum gravity potential) or the floor (Figs. 1 (b), (c)).
4. Then, return to Step 1 and repeat the process until the RVE is filled with particles.

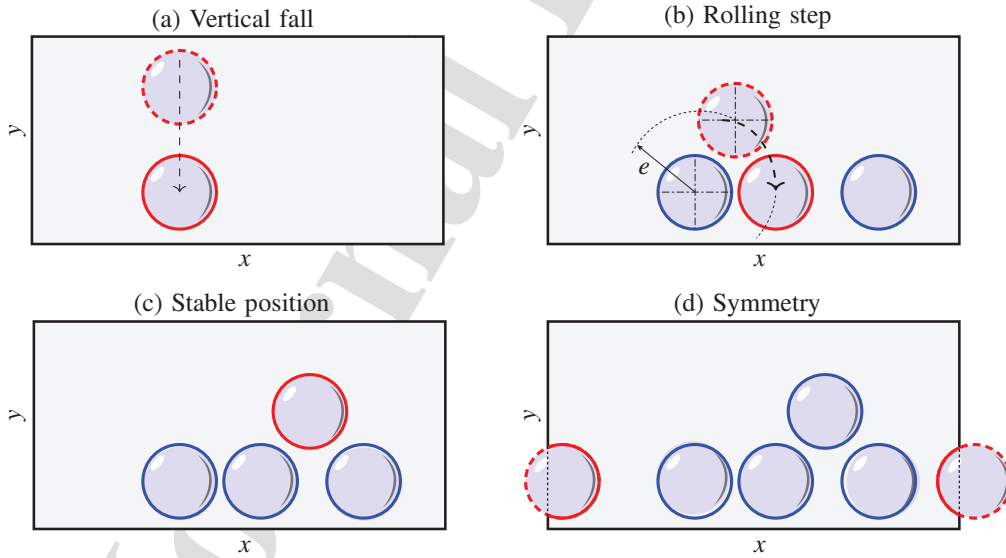


Figure 1: Outline of the dropping and rolling algorithm for 2D RVEs.

In the 3D framework the process is similar, but in the rolling step different possibilities must be taken into account, depending on whether the falling particle comes into contact with one, two or three spheres [46]. In the first case, the sphere rolls in the same way as in the two-dimensional case. In the second case, the particle rolls

in the direction defined by the plane normal to the vector joining the centres of the contact spheres. In the last one, the incoming sphere moves on the two spheres on which it rolls down most steeply until it reaches a stable position. Additionally, to impose periodic boundary conditions as explained hereafter, the geometric periodicity of the RVE is imposed. To do so, two different approaches are commonly adopted in the literature either inclusions are allowed or not to cut the boundaries of the RVE. The second approach is adopted in this work since, while the implementation becomes more involved, the resulting RVEs are more realistic. To this aim, any particle that intersects any of the vertical walls or corners of the RVE is replicated at the opposite wall or corner (see Figs. 1(d) and 2). Such a process can be described in the more complex case of 3D RVEs by the following procedure:

1. Consider a particle in stable position with centre's coordinates  $(x, y, z)$ . This centre is allowed to partially fall outside of the RVE.
2. Check if the particle intersects any of the surfaces of the cell. If so, symmetric particles -one, three or seven, depending if the original one cuts one, two or three cell faces, respectively- are generated in order to impose periodicity (see Fig. 1 (d)).
3. Check if any of the generated particles in the previous step overlap the previous existing ones. If this is not the case, the proposal particle is accepted, otherwise return to Step 1.
4. Repeat until the desired filler volume fraction is achieved.

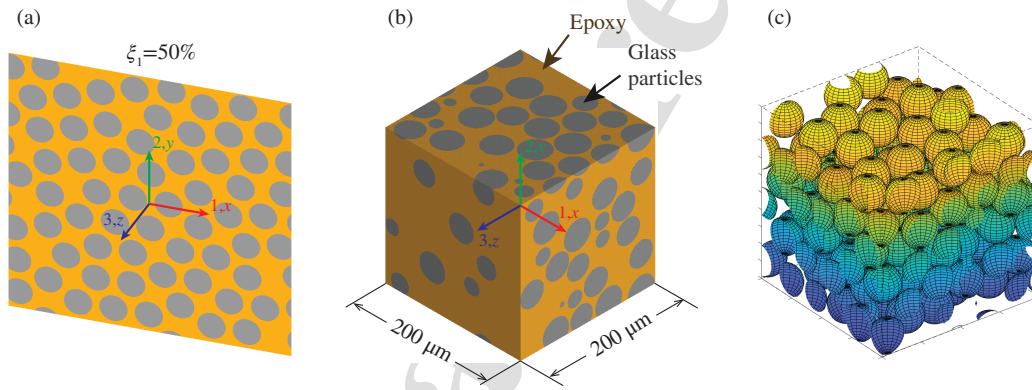


Figure 2: (a) Example of a periodic  $200 \mu\text{m}$  edge 2D RVE matrix doped with  $\xi_1 \approx 50\%$  of glass particles with radius  $10 \mu\text{m}$ . (b) RVE doped with  $\xi_1 \approx 50\%$  volume fraction of glass microspheres with radius  $20 \mu\text{m}$ . (c) Example of a 3D RVE generated particle distribution by means of the rolling and dropping procedure with  $\xi_1 \approx 50\%$ .

For the 2D specimen  $\Omega \subset \mathbb{R}^2$ , a completely analogous procedure can be implemented. In either case, the final filler volume fraction  $\xi_1$  is directly determined by the inter-particle distance parameter  $e$  and the diameter of the particles. In order to provide a simple expression for the relationship between the ratio  $e/r$  and the resulting volume fraction  $\xi_1$ , a Monte Carlo analysis with 300 different geometries has been conducted in a RVE with  $L = 300 \mu\text{m}$  with four different particles' radii  $r$ , namely  $r = 7.5, 10, 15,$  and  $25 \mu\text{m}$  for 2D case and  $r = 10, 15, 25,$  and  $50 \mu\text{m}$  for 3D. Figure 3 shows the obtained volume fractions versus the ratio  $e/r$ . It is noted in this figure that a common trend is found for all the cases thanks to the non-dimensionalization of the results. Only some instabilities are observed for large particle sizes. In this light, new expressions for the filler volume fraction are obtained by curve fitting of the results in Fig. 3 as  $\xi_1 = 3.2(e/r)^{-2}$  and  $\xi_1 = 4.5(e/r)^{-3}$  for 2D and 3D RVEs, respectively. Note that the implemented algorithm achieves filler volume fractions up to 50%.

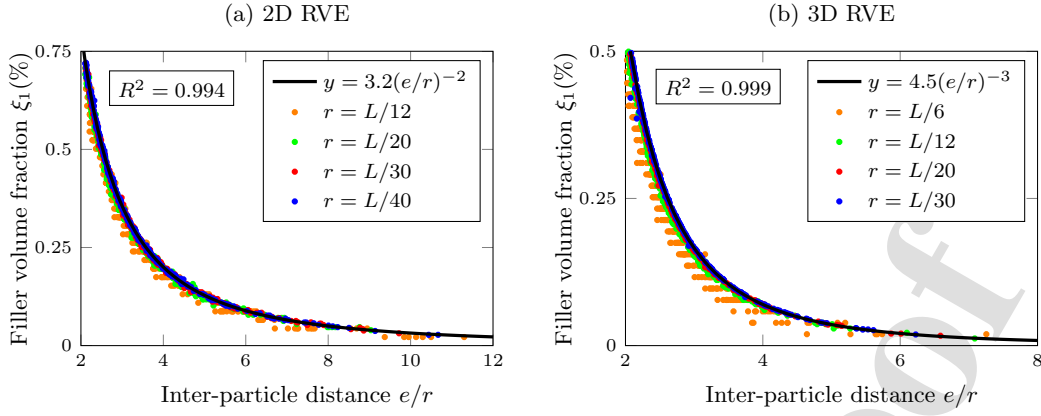


Figure 3: Relationship between the filler volume fraction  $\xi_1$  and the ratio between the inter-particle distance parameter  $e$  and the radius of the particles  $r$  for 2D and 3D RVEs.

Once the RVE is defined, its effective elastic properties are obtained in this work by applying periodic boundary conditions as anticipated above. The enforcement of geometrical periodicity implies that the composite material can be conceived as the periodic replication of the RVE (Fig. 4 (a)). The general periodic boundary conditions on the cell faces of a RVE are given by [47]:

$$u_i = \hat{\epsilon}_{ij}x_j + v_i, \quad (6)$$

where  $\hat{\epsilon}_{ij}$  denote the volume average strains, and  $v_i$  represents the local periodic part of the displacement components  $u_i$  on the boundary surfaces. The latter displacement components are generally unknown and depend upon the applied loading. Indices  $i$  and  $j$  denote the global Cartesian directions. In the case of square RVEs like the ones used in this work and sketched in Fig. 4 (a), Eq. (6) takes a more explicit expression. Consider the notation of the cell surfaces  $A^-/A^+$ ,  $B^-/B^+$ , and  $C^-/C^+$  shown in Fig. 4 (a).

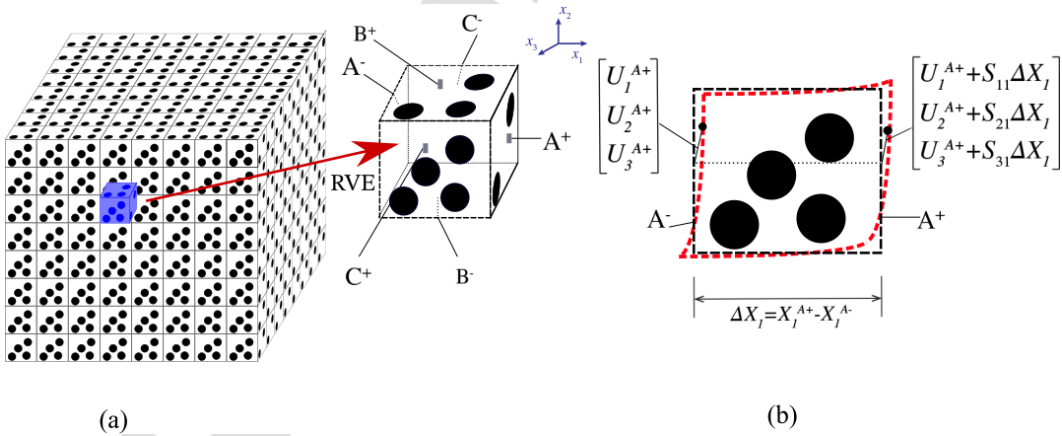


Figure 4: (a) Representation of a periodic composite and definition of the RVE. (b) Periodic boundary conditions for a pair of nodes located on the opposite surfaces  $A^-$  and  $A^+$ .

Then, the displacements on a pair of opposite boundary cells (with their normal along the  $x_j$  axis) read:

$$u_i^{K+} = \hat{\varepsilon}_{ij} x_j^{K+} + v_i^{K+}, \quad u_i^{K-} = \hat{\varepsilon}_{ij} x_j^{K-} + v_i^{K-}, \quad (7)$$

where indexes  $K+$  and  $K-$  indicate the displacements along the positive and negative  $x_j$  directions, respectively. Local fluctuations  $v_i^{K-}$  and  $v_i^{K+}$  must be identical on every two opposing faces to comply with the periodicity of the RVE. Therefore, the local displacement components can be dropped from the formulation by the difference between the expressions in Eq. (7), leading to:

$$u_i^{K+} - u_i^{K-} = \hat{\varepsilon}_{ij} (x_j^{K+} - x_j^{K-}). \quad (8)$$

Therefore, the RVE can be subjected to a desired strain state by imposing proper displacements on its boundary surfaces. Then, the volume average stresses  $\hat{\sigma}_{ij}$  and strains  $\hat{\varepsilon}_{ij}$  in the RVE can be computed as:

$$\hat{\varepsilon}_{ij} = \frac{1}{\mathcal{V}} \int_{\mathcal{V}} \varepsilon_{ij} d\mathcal{V}, \quad \hat{\sigma}_{ij} = \frac{1}{\mathcal{V}} \int_{\mathcal{V}} \sigma_{ij} d\mathcal{V}, \quad (9)$$

with  $\mathcal{V}$  being the volume of the RVE. Then, the  $ij$ -th component of the elastic tensor can be directly estimated as  $\mathbf{C}_{ij}^* = \hat{\sigma}_{ij} / \hat{\varepsilon}_{ij}$ .

### 3. Adaptive PCE surrogate modelling

Denote by  $\mathcal{M}^*$ , with  $*$  = 2D, 3D, the numerical homogenisation models of representative 2D/3D RVEs. Assuming the microstructural properties of interest as independent random variables arranged in a vector  $\mathbf{X} = (X_1, X_2, \dots, X_M)$ ,  $\mathcal{M}^*$  maps a  $M$ -dimensional input parameter space to a 1-dimensional output space  $\mathcal{M}^* : \mathbb{R}^M \rightarrow \mathbb{R}$ . Due to the presence of uncertainties in the input vector,  $\mathbf{X}$  is considered a random variable with known probability distribution. Then, a surrogate model  $\hat{\mathcal{M}}^*$  aims to emulate the original homogenisation model  $\mathcal{M}^*$ , but at a lower computational cost. The general procedure to construct a surrogate model can be summarized in the following steps:

1. Sample two independent input data sets: the *training set* (TS)  $T$  and the *validation set* (VS)  $V$  covering the parameter design space:

$$T = \{\mathbf{X}^{(1)}, \dots, \mathbf{X}^{(N)}\} \subset \mathbb{R}^{M \times N}, \quad V = \{\mathbf{X}^{(1)}, \dots, \mathbf{X}^{(K)}\} \subset \mathbb{R}^{M \times K}. \quad (10)$$

2. Evaluate model  $\mathcal{M}^*$  on set  $T$ .
3. Solve an optimization problem to identify the parameters of the surrogate model.
4. Assess the metamodel's accuracy by evaluating  $\mathcal{M}^*$  and  $\hat{\mathcal{M}}^*$  on set  $V$ .

In this study, PCE is adopted for its convenience to represent stochastic magnitudes of interest. In particular, PCE is used to represent the effective elastic properties  $y$  obtained by numerical homogenisation through an expansion onto an orthogonal multivariable polynomial basis [16] as:

$$y = \mathcal{M}^*(\mathbf{X}) = \sum_{\alpha \in \mathbb{N}^M} a_\alpha \Psi_\alpha(\mathbf{X}), \quad \alpha = (\alpha_1, \dots, \alpha_M), \quad \alpha_i \in \mathbb{N}, \quad (11)$$

where:

- $\Psi_{\alpha}(\mathbf{X}) = \prod_{i=1}^M \psi_{\alpha_i}^{(i)}(X_i)$  are multivariate polynomials.
- $\psi_{\alpha_i}^{(i)}$  are orthogonal polynomials depending on the stochastic nature of the input variables  $\mathbf{X}$ . In this work, Legendre and Hermite polynomials will be used to represent uniform and gaussian distributions.

Although expression (11) can be proved exact for an infinite number of polynomials, in practice only a finite number of terms in  $\sum_{\alpha \in \mathbb{N}^M} a_{\alpha} \Psi_{\alpha}(\mathbf{X})$  can be computed. As a consequence, different strategies can be taken into account to truncate the polynomial series. The simplest one consists in selecting all the polynomials whose total degree  $|\alpha| = \sum_{i=1}^M \alpha_i$  belongs to the set:

$$\mathcal{A}^{M,p} = \{\alpha \in \mathbb{N}^M : 0 \leq |\alpha| \leq p\}, \quad (12)$$

where the cardinality of  $\mathcal{A}^{M,p}$  is equal to:

$$\binom{M+p}{p} = \frac{(M+p)!}{M!p!}. \quad (13)$$

Nonetheless, when  $M$  and  $p$  are large enough, this procedure of polynomial selection may lead to computing a large number of coefficients and the subsequent computational burden. As an alternative, an hyperbolic truncation scheme can be employed. This approach consists in selecting all multi-indices with  $q$ -norm [48]

$$\|\alpha\|_q = \left( \sum_{i=1}^M \alpha_i^q \right)^{\frac{1}{q}},$$

less or equal to  $p$ , i.e.:

$$\mathcal{A}^{M,p,q} = \{\alpha \in \mathbb{N}^M : \|\alpha\|_q \leq p\}. \quad (14)$$

This strategy has been proved efficient due to the fact that high interaction terms often have coefficients close to zero. Nonetheless, although substantial cost reductions can be achieved using the hyperbolic truncation scheme, the number of coefficients in the expansion may still be considerable. A better cost-efficient solution can be obtained by using the adaptive LAR algorithm [49]. LAR constructs a set of expansions incorporating an increasing number of basis polynomials  $\Psi_{\alpha}$ , from 1 to  $\mathcal{P} = \text{card}(\mathcal{A}^{M,p,q})$ . Then, the resulting sequence of index sets is used to construct different expansions and the best meta-model is selected by a cross validation procedure. Finally, the expansion coefficients  $\mathbf{a} = \{a_{\alpha}, \alpha \in \mathcal{A}^{M,p} \subset \mathbb{N}^M\}$  are obtained by minimizing the expectation of the least squares errors:

$$\hat{\mathbf{a}} = \arg \min_{\mathbf{a} \in \mathbb{R}^{\mathcal{P}}} \frac{1}{N} \sum_{i=1}^M \left[ \mathcal{M}^*(\mathbf{X}^{(i)}) - \sum_{\alpha \in \mathcal{A}} a_{\alpha} \Psi_{\alpha}(\mathbf{X}^{(i)}) \right]^2, \quad (15)$$

where  $\mathbf{X}^{(i)} \in T$ ,  $i = 1, \dots, N$ . Once Eq. (15) has been solved, the resulting PCE surrogate model can be written as follows:

$$y = \mathcal{M}^*(\mathbf{X}) \approx \hat{\mathcal{M}}^*(\mathbf{X}) = \sum_{\alpha \in \mathcal{A}} \hat{a}_{\alpha} \Psi_{\alpha}(\mathbf{X}). \quad (16)$$

#### 4. Surrogate model-based uncertainty propagation analysis of composite materials

The main contribution of this section regards the application of the previously introduced surrogate modelling approach to the analysis of the propagation of uncertainties in the material parameters through the homogenization of both 2D/3D composites with high filler volume fraction. The general methodology is sketched in Fig. 5 and includes five main steps, namely (i) geometry construction using the dropping and rolling method, (ii) design of proper RVEs, (iii) construction of the metamodels, (iv) validation and (v) uncertainty propagation analysis.

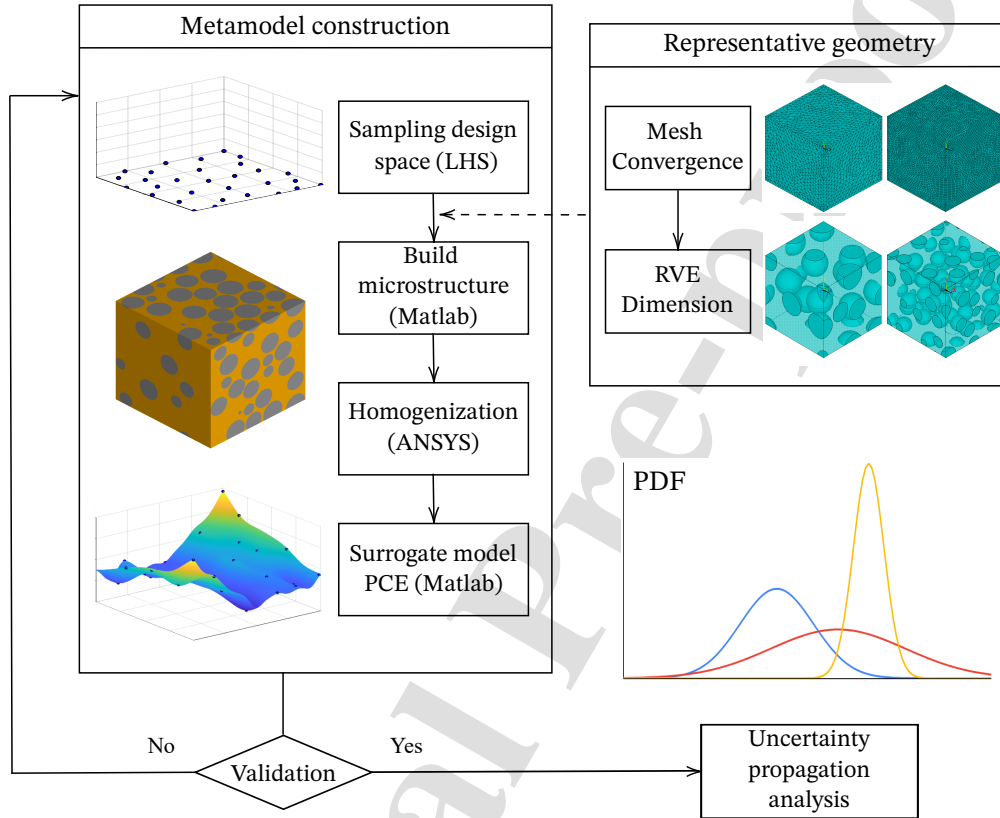


Figure 5: Flowchart of the proposed meta-model approach to perform uncertainty propagation analysis in 2D/3D homogenisation.

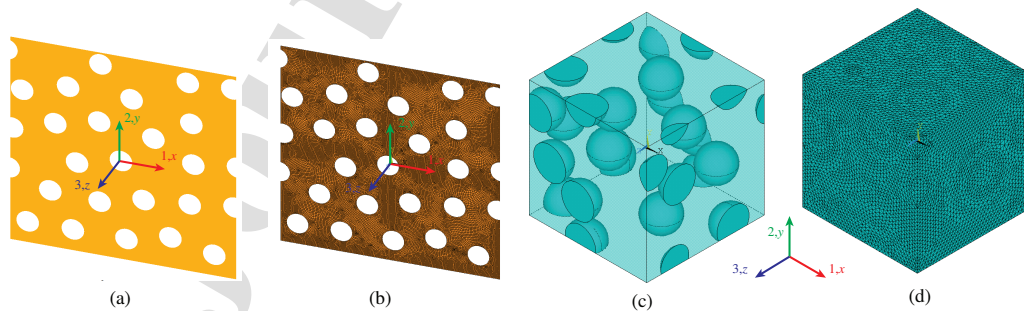


Figure 6: (a) Matrix and (b) meshed matrix of an example of a periodic 200  $\mu\text{m}$  edge 2D RVE of epoxy doped with  $\xi_1 \approx 20\%$  volume fraction of spherical particles. (c) RVE with a length side of 200  $\mu\text{m}$  doped with  $\xi_1 \approx 15\%$  volume fraction of glass microspheres (d) and corresponding FEM mesh (90443 nodes).

In a first step, general 2D/3D quadratic and cubic models allowing particle intersection with the cell boundaries (Fig. 2) are implemented. For the construction and homogenisation of the microstructure, a combination of scripts generated in MATLAB environment [50] and the commercial FEM tool ANSYS is used [51]. Specifically, the adopted methodology for defining the geometry of cubic RVEs involves the steps previously given in Section 2. Once the geometry is constructed, it is discretized in ANSYS using plane-strain 8-nodes quadratic elements (PLANE 183) for 2D RVEs, while 4-nodes linear tetrahedral solid elements (SOLID 285) are used for 3D RVEs. Two samples of the generated RVEs are shown in Figs. 6 (a), (c) along with their corresponding meshes in Figs. 6 (b), (d). Once constructed, the numerical homogenisation model is used to draw the samples of the training and validation sets for the construction of the surrogate model.

To assess the precision of the developed surrogate models, both local and global error metrics are considered. These include the coefficient of determination  $R^2$  and the Normalized Average Absolute Error (NAAE) for the global accuracy and the Normalized Maximum Absolute Error (NMAE) for the local case, are reported in Table 1, where  $\bar{y}$  denotes the arithmetic mean of the validation output set. These global metrics are evaluated over two data sets  $\{y^{(1)} = \mathcal{M}(\mathbf{X}^{(1)}), \dots, y^{(K)} = \mathcal{M}(\mathbf{X}^{(K)})\}$  and  $\{\hat{y}^{(1)} = \hat{\mathcal{M}}^*(\mathbf{X}^{(1)}), \dots, \hat{y}^{(K)} = \hat{\mathcal{M}}^*(\mathbf{X}^{(K)})\}$  obtained, respectively, by the evaluation of the numerical homogenisation models and their corresponding meta-models over the VS with  $K$  realisations.

Table 1: Error metrics for the accuracy assessment of surrogate models over a validation set of size  $K$ .

Coefficient of Determination ( $R^2$ )	Normalized average absolute error (NAAE)	Normalized maximum absolute error (NMAE)
$R^2 = 1 - \frac{\sum_{i=1}^K (\hat{y}^{(i)} - y^{(i)})^2}{\sum_{i=1}^K (\bar{y} - y^{(i)})^2}$	$NAAE = \frac{\sum_{i=1}^K  \hat{y}^{(i)} - y^{(i)} }{K \sqrt{\frac{1}{K-1} \sum_{i=1}^K (\bar{y} - y^{(i)})^2}}$	$NMAE = \frac{\max_{i=1}^K  \hat{y}^{(i)} - y^{(i)} }{K \sqrt{\frac{1}{K-1} \sum_{i=1}^K (\bar{y} - y^{(i)})^2}}$

Once constructed, PCE sensitivity analysis (SA) is used to investigate the contribution (relative importance) of each random input parameter of the mathematical model  $\mathcal{M}$  to its stochastic response. The non-linearity of the proposed model implies that not only the variables individually affect the response, but also the interactions between them. Therefore, the joint-effect of parameter variation must be also quantified. Sobol' indices [43] represent a global SA method as they provide the sensitivity of the predictions of the surrogate model to variations in the selected input variables. The Sobol' index  $S_u$  associated to the subset  $\mathbf{u} = \{i_1, \dots, i_M\} \subset \{1, \dots, M\}$  is defined as the ratio between the contribution to the model variance given by the interaction among the components of  $\mathbf{u}$  and the total variance. Thanks to the orthogonality of the PCE, it can be written as:

$$S_u = \left( \sum_{\alpha \in \mathcal{A}_u} a_\alpha^2 \right) / \left( \sum_{\alpha \in \mathcal{A}} a_\alpha^2 \right), \quad \mathcal{A}_u = \{\alpha \in \mathcal{A} : \alpha_k \neq 0 \text{ when } k \in \mathbf{u}\}. \quad (17)$$

## 5. Numerical results and discussion

This section presents the numerical results and discussion obtained by applying the previously introduced methodology for the uncertainty propagation analysis of epoxy composites doped with glass fiber spherical particles with a wide range of filler concentrations (from 0% up to 50 %). The presented results are organised as follows: Section 5.1 presents preliminary convergence analyses conducted to identify the minimum RVE's sizes

and mesh densities. Section 5.2 reports the construction of the surrogate models and their quality assessment. Finally, Section 5.3 reports the surrogate model-based uncertainty propagation analyses by introducing uncertainties in the elastic properties of the micro-constituents. In the following analyses, the material properties of epoxy and glass spheres are taken from reference [52] as listed in Table 2.

Table 2: Mechanical properties of the constituent phases of epoxy doped with glass fiber micro-spheres [52].

	Epoxy polymer	Glass fiber particles
Young's Modulus [GPa]	3.0	76.0
Poisson's ratio [-]	0.4	0.23
Radius [ $\mu\text{m}$ ]	-	8 – 20

### 5.1. Convergence analysis of the RVEs' sizes and mesh density

To guarantee that a RVE statistically represents the composite material, its dimension and the number of embedded particles must be carefully selected. In addition, since the microstructure is then discretized using FEM, another important aspect to determine regards the mesh density. In general, the dimensions of the RVE and its mesh density must be chosen as a trade-off between representativity and computational cost. Firstly, the discretization of the RVEs is selected fine enough to ensure that the homogenised constitutive tensor  $\mathbf{C}^*$  is mesh independent. On the other hand, the dimensions of the RVE are selected according to the degree of isotropy of the obtained constitutive tensor. Given that both matrix phase and reinforcing particles are isotropic, spherical, and randomly dispersed, the resulting effective constitutive tensor must also present isotropic symmetry. In this light, Fig. 7 reports the convergence analysis of two 2D meshes with edge lengths of 120  $\mu\text{m}$  and 240  $\mu\text{m}$ . In both cases, a filler volume fraction of 20% has been selected. In this figure, the effective Young's moduli  $E_x$ ,  $E_y$  are presented versus the total number of nodes in the mesh ( $xyz$  reference frame indicated in Fig. 6). Five different meshes with increasing densities have been considered, including 2116, 7592, 11555, 22304, 43776 nodes for the 120  $\times$  120  $\mu\text{m}$  RVE and 15086, 27515, 43388, 83531, 111512 for the 240  $\times$  240  $\mu\text{m}$  one. It is noted in this figure that convergence is approximately achieved between the third and the fourth discretization densities (22000-83500 nodes, mean element edge size 1.32% the RVE size). Therefore, the fourth mesh density is selected as a conservative solution. These analyses were also conducted for 3D RVEs, achieving similar conclusions (mean element edge size 1.11% the RVE size).

Once the mesh density has been defined, the size of the RVEs is selected by convergence analysis of the isotropy degree of the effective constitutive tensor. To do so, five geometries with different RVE sizes have been studied, namely 80, 120, 160, 200 and 240  $\mu\text{m}$  (80, 120, 160 and 200  $\mu\text{m}$  in 3D) have been studied. The convergence analysis of the effective Young's moduli  $E_i$  obtained for 2D and 3D RVEs are shown in Figs. 8 and 9, respectively. Moreover, the evolution of the mean Poisson's ratios  $\{v_{xy}\}$  and  $\{v_{xy}, v_{xz}, v_{yz}\}$  obtained by 2D and 3D RVEs are also reported in Figs. 10 (a) and (b), respectively. In the ideal case of perfect isotropy, ratios  $E_i/E_j$  should be exactly equal to 1. Therefore, following Figs. 8 (a) and 9 (a,b,c), it can be concluded that convergence is approximately achieved for RVEs with an edge length of 240  $\mu\text{m}$  in 2D and 200  $\mu\text{m}$  in 3D. In these cases, it is noted that the ratios between the elastic moduli are very close to 1.

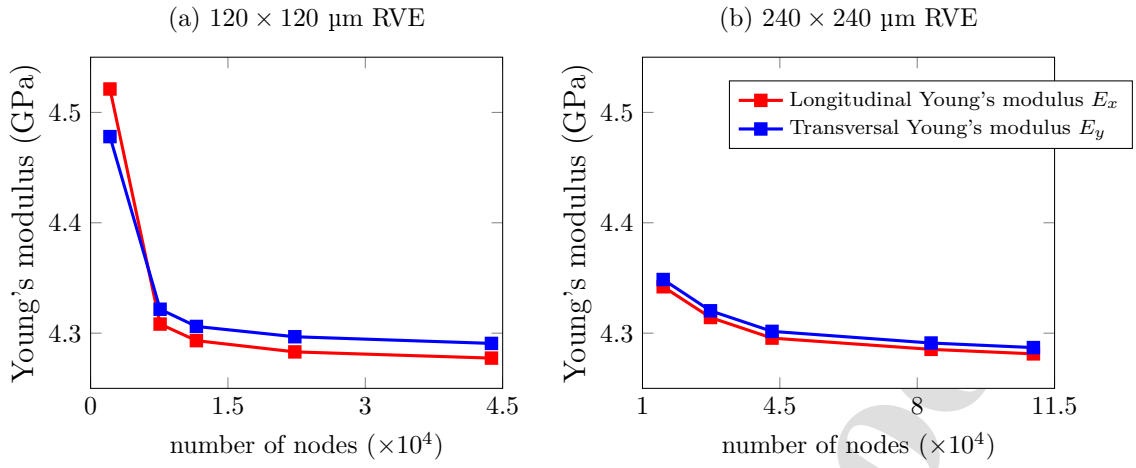


Figure 7: Convergence analysis of the mesh density for a 2D RVE of dimensions  $120 \times 120 \mu\text{m}$  (a) and  $240 \times 240 \mu\text{m}$  (b) doped with 20% volume fraction of spherical particles with radius  $8 \mu\text{m}$ .

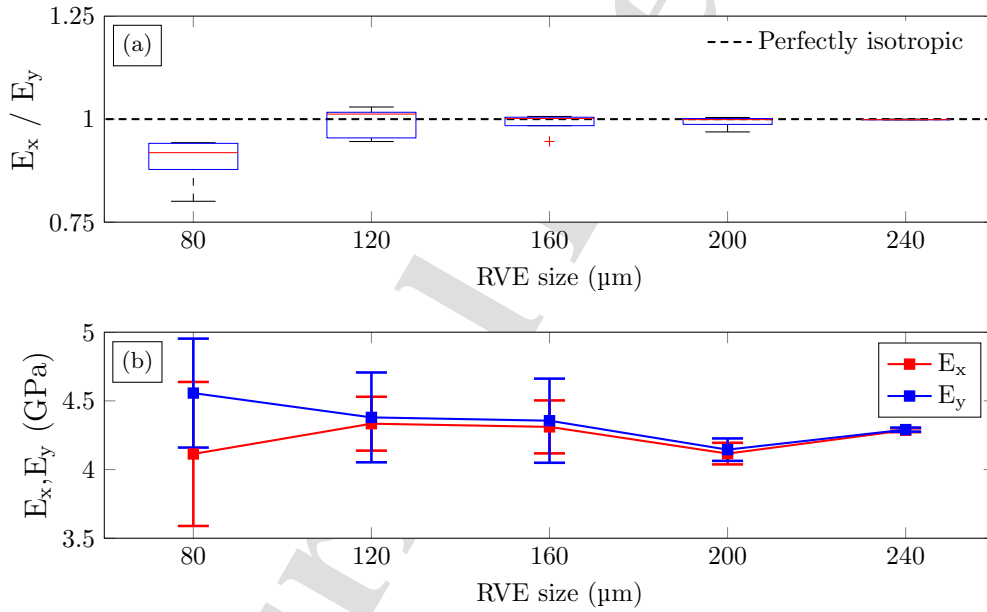


Figure 8: Analysis of the isotropy of the composite (a) and evolution of the elastic Young's moduli  $E_x, E_y$  with error bars denoting the standard deviation (b) against the length side of the 2D RVE. (Filler volume fraction  $\xi_1 = 20\%$ )

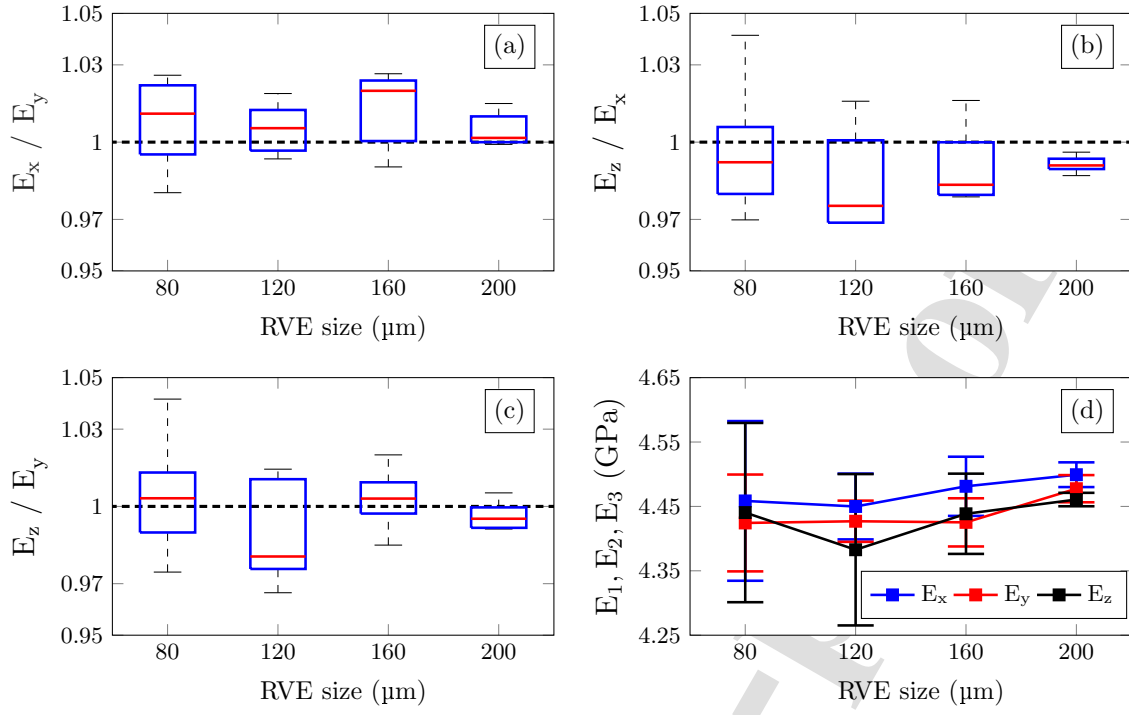


Figure 9: Analysis of the isotropy of the composite in terms of the ratio between the Young moduli (a)  $E_x/E_y$ , (b)  $E_z/E_x$ , (c)  $E_z/E_y$  and (d) evolution of the mean Young's moduli  $E_x$ ,  $E_y$ ,  $E_z$  against the length side of the 3D RVE for a volume fraction  $\xi_1 = 0.2$  (error bars in (d) denote standard deviation).

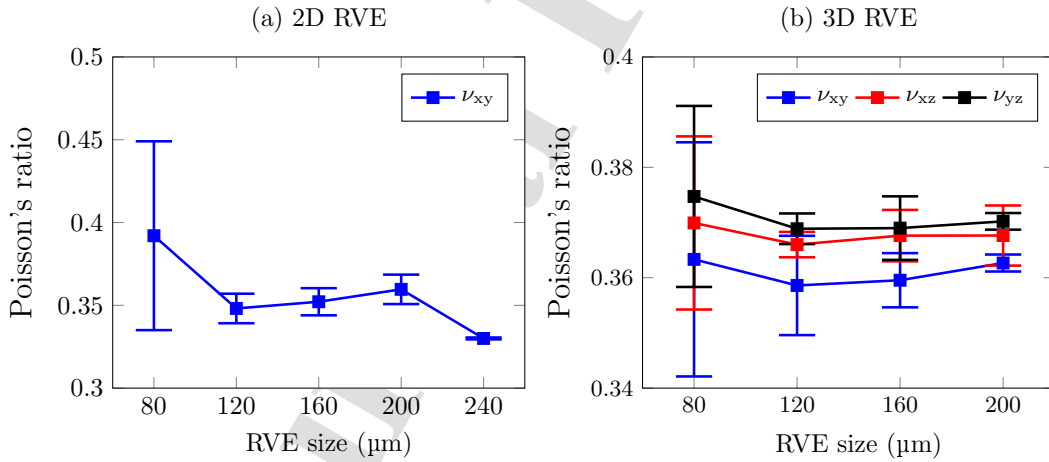


Figure 10: Convergence analysis of the mean effective Poisson's ratios  $\{\nu_{xy}\}$  and  $\{\nu_{xy}, \nu_{xz}, \nu_{yz}\}$  obtained by 2D (a) and 3D RVEs (b) against the RVE size for a filler volume fraction of  $\xi_1 = 0.2$ . Error bars stand for standard deviations.

The previous analyses are further investigated in Fig. 11, which reports the mean values of the main components of the effective constitutive tensor  $\mathbf{C}^*$  obtained for five realizations of the RVEs with increasing sizes. In light with the previous analyses, it is observed in this figure that the composites exhibit a higher degree of isotropy as the RVE size increases. For instance, note in Figs. 11 (a) and (c) that the components  $C_{ii}$  (diagonal terms of

the constitutive tensor) tend to a common value as expected for isotropic materials. The residual anisotropy in the effective constitutive tensor is eliminated hereafter through integration over all possible orientations in the Euler space, also referred to as the orientational average. To do so, tensor  $\mathbf{C}^*$  is rotated to any orientation in the Euler space as  $C_{ijkl} = a_{ip}a_{jq}a_{kr}a_{ls}C_{pqrs}^*$ , where  $\mathbf{a}$  is the transformation matrix consisting of  $\theta$ ,  $\phi$ , and  $\psi$  rotation angles. Then, the orientational average of  $\mathbf{C}^*$  can be obtained as [53]:

$$\langle \mathbf{C}^* \rangle = \frac{1}{4\pi^2} \int_0^{2\pi} \int_0^{2\pi} \int_0^{\pi/2} \mathbf{C}^*(\theta, \phi, \psi) \sin \theta d\theta d\phi d\psi. \quad (18)$$

On this basis, the effective elastic modulus  $E$  and Poisson's ratio  $\nu$  can be obtained from the compliance tensor  $\mathbf{S} = (\mathbf{C}^*)^{-1}$  in Mandel-Voigt notation as

$$E = \frac{1}{S_{11}}, \quad \nu = -ES_{12}. \quad (19)$$

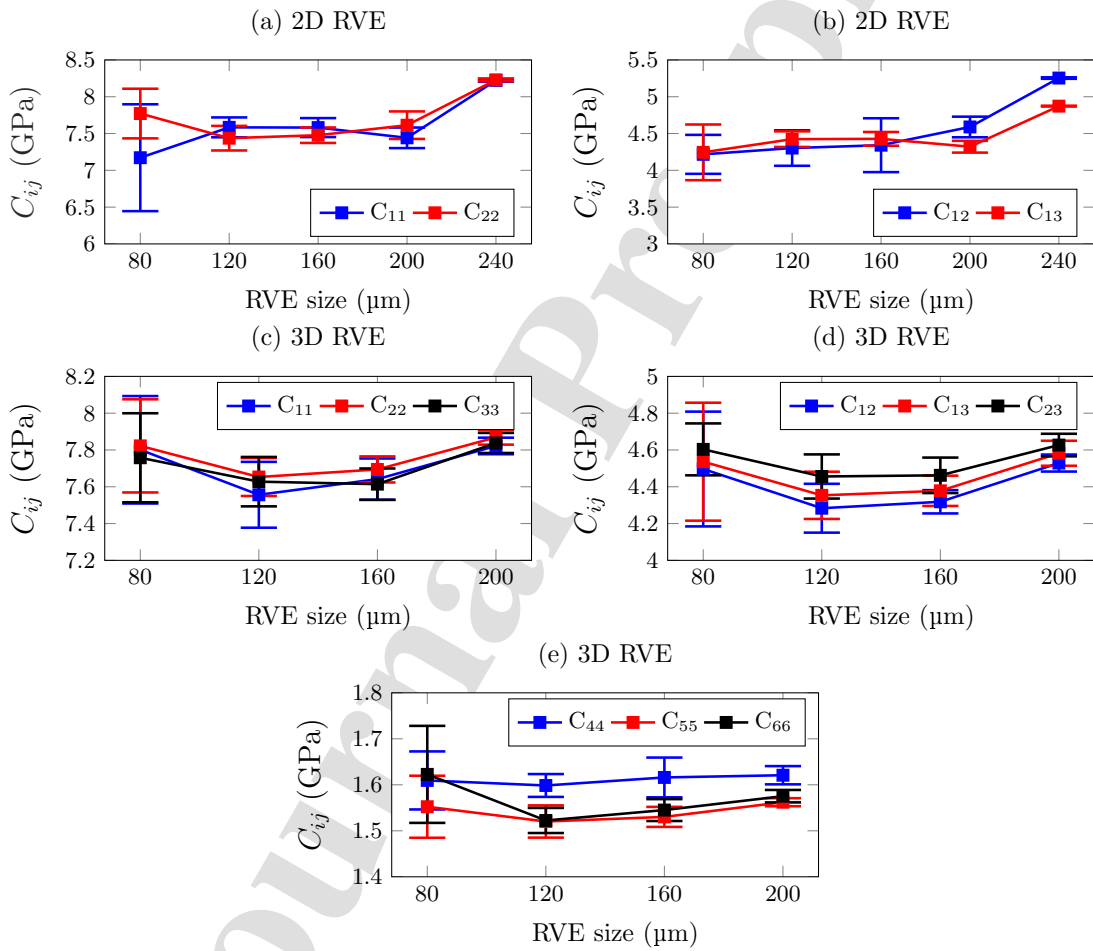


Figure 11: Convergence analysis of the mean effective constitutive tensor components  $\{C_{ij}\}$  by 2D (a,b) and 3D RVEs (c,d,e) against the RVE size for a filler volume fraction of  $\xi_1 = 0.2$ . Error bars stand for standard deviations.

### 5.2. Surrogate model construction. Accuracy, sensitivity analysis and computational efficiency

Following the theoretical framework introduced in Section 3, to approximate the 2D/3D homogenised Young's moduli, two PCE surrogate models  $\hat{\mathcal{M}}^{2D}$  and  $\hat{\mathcal{M}}^{3D}$  have been constructed taking  $p = 0.95$  in Eq. (14) and model

orders between 1 and 4. To this purpose, 50 training points and 25 independent validation points have been considered by means of the Latin Hypercube Sampling (LHS) [54] procedure. Five input variables have been included in both models, namely the Young's moduli and Poisson's ratios of the matrix and the inclusions, as well as the filler volume fraction. Uncertainties in the elastic properties of the constituents are assumed normally distributed with mean values from Table 2 and standard deviations corresponding to 1/30 of mean values (corresponding deviations of up to  $\pm 10\%$  of them). On the other hand, the filler volume fraction is assumed uniformly distributed within the range from 0 to 50%. The selected probability distributions are collected in Table 3.

Table 3: Statistical distributions of the material parameters.

Variable	Notation	Distribution
Young's modulus of epoxy matrix [GPa]	$E_0$	Gaussian $\mathcal{N}(3, 0.1)$
Poisson's ratio of epoxy matrix [-]	$\nu_0$	Gaussian $\mathcal{N}(0.4, 0.0133)$
Young's modulus of glass reinforcement [GPa]	$E_1$	Gaussian $\mathcal{N}(76, 2.5333)$
Poisson's ratio of glass reinforcement [-]	$\nu_1$	Gaussian $\mathcal{N}(0.23, 0.0076)$
Volume fraction of inclusions [-]	$\xi_1$	Uniform $\mathcal{U}(0, 0.5)$

The performance assessment of the developed surrogate models through the error metrics from Table 1 as well as the computational time savings are reported in Table 4. It can be noted in this table that the surrogate models  $\hat{\mathcal{M}}^{2D}$  and  $\hat{\mathcal{M}}^{3D}$  faithfully reflect the behaviour of the corresponding parent models  $\mathcal{M}^{2D}$  and  $\mathcal{M}^{3D}$ . This coincides with Fig. 12 which shows a comparison between them and the forward FEM over the 25 samples of the validation set. The low scatters of the points around the diagonal lines and the coefficients of determination (very close to 1) corroborate that the surrogate models are formed with accuracy. With respect to the computational times, it is important to remark that, while the numerical homogenisation models  $\mathcal{M}^{3D}$  and  $\mathcal{M}^{2D}$  take around 6 hours and several minutes, respectively, the evaluation of the respective meta-models ( $\hat{\mathcal{M}}^{3D}$ ,  $\hat{\mathcal{M}}^{2D}$ ) takes less than 1 millisecond (99.7% reduction). Based on the metrics in Table 4 and the fact that 2D and 3D models provide similar results for moderate volume fractions, 2D approximations may be adopted in these cases for fast evaluations with reasonably good accuracy. Finally, Table 5 reports the Sobol' indices of the constructed expansions. As it is expected, the homogenisation results are particularly sensitive to the filler's volume fraction contribution followed by the properties of the matrix.

Table 4: Surrogate model accuracy.

	$R^2$	NAAE ( $10^{-2}$ )	NMAE ( $10^{-2}$ )
$\hat{\mathcal{M}}^{2D}$	0.9939	5.34	0.84
$\hat{\mathcal{M}}^{3D}$	0.9993	2.15	0.40

Table 5: Sobol' indices.

	$S_{\xi_1}$	$S_{E_0}$	$S_{\nu_0}$	$S_{E_1}$	$S_{\nu_1}$
$\hat{\mathcal{M}}^{2D}$	0.9913	0.0075	0.0031	$1.7021E - 5$	0
$\hat{\mathcal{M}}^{3D}$	0.9831	0.0086	0.0130	0	0

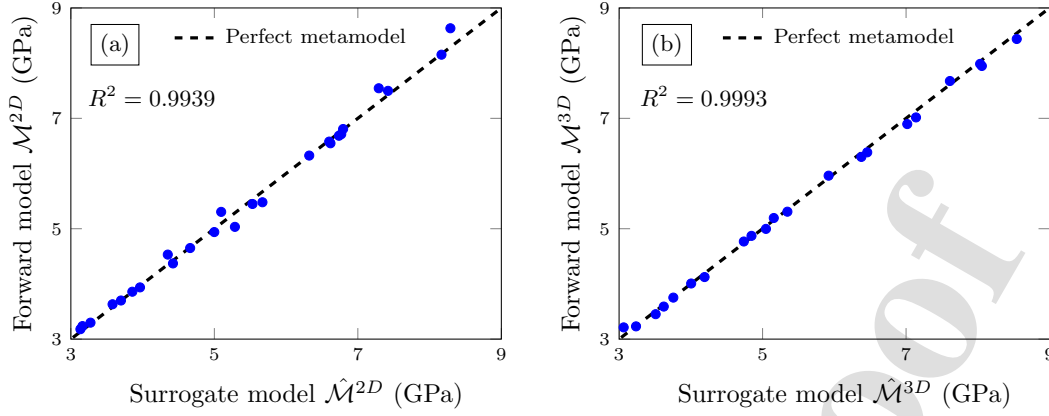


Figure 12: Comparison of the numerical estimates by FEM and the predictions of the PCE surrogate models in terms of the elastic moduli in (a) 2D and (b) 3D cases.

### 5.3. Uncertainty propagation analyses. Comparison between the 2D and 3D surrogate approximations.

The accuracy and computational efficiency of the developed surrogate models are leveraged herein to analyse the propagation of uncertainties in the microstructural properties of epoxy/glass composites upon the effective elastic properties. Firstly, uncertainty propagation analyses are conducted by considering isolated uncertainties in every of the considered microstructural parameters. In each analysis, 25000 Monte Carlo individuals are drawn by sampling from the statistical distribution of the parameter under analysis as reported in Table 3, while the remaining parameters are fixed to their mean values. It is important to remark that the simulations took less than 1 second, while conducting such analyses using the numerical homogenisation model would be simply infeasible. Once the Monte Carlo samples are obtained, the statistical distributions of the effective elastic properties are estimated in frequentist terms. Following this, Fig. 13 represents the probability distribution functions (PDFs) of the considered parameters in the expansions for the 2D/3D surrogate models. In both 2D and 3D scenarios, Fig. 13 shows that for low filler volume fractions, uncertainties in  $E_0$  dominate the uncertainty of the effective Young's modulus. Nonetheless, almost no effect is observed for variations in the elastic modulus of the glass inclusions and the remaining parameters. It is also noted that for higher filler volume fractions, some influence is found due to uncertainty in the Poisson's ratio of the host matrix.

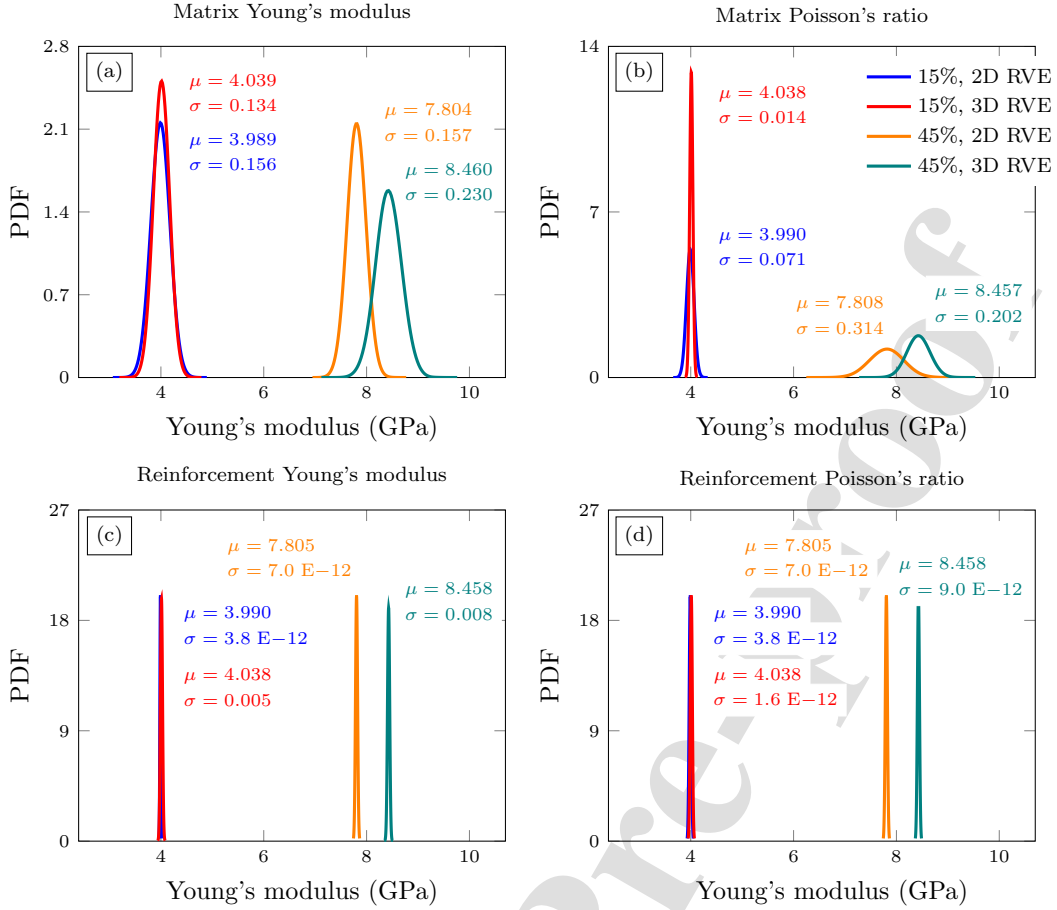


Figure 13: PDFs of elastic properties of 2D and 3D composites made of epoxy doped with 15% and 45% of glass fiber inclusions considering uncertainties in the matrix Young's modulus (a), in the matrix Poisson's ratio (b), in the glass reinforcement Young's modulus (c) and in the glass reinforcement Poisson's modulus (d).

Finally, Fig. 14 presents the statistical probability distribution functions (PDFs) of the effective elastic moduli of 2D/3D glass fiber/epoxy composites when considering simultaneous uncertainty in all the considered microstructural parameters. The analyses are conducted for two filler volume fractions, namely 15% and 45%. It is shown in this figure that, for the filler volume fraction of 15%, the mean values of the elastic moduli predicted by the 2D and the 3D models are almost identical. However, as the volume fraction increases, increasing differences arise. For example, it is noted in Fig. 14 that for a filler volume fraction of 45%, the mean values of the Young's moduli predicted by the 2D and the 3D model are around 7.807 GPa and 8.459 GPa, respectively.

In order to provide further insight into the uncertainty propagation characteristics of the elastic moduli of glass fiber/epoxy composites, Fig. 15 reports a scatter plot of the Monte Carlo samples of the effective elastic modulus for filler volume fractions up to 50%. In this figure, the 95% confidence levels are indicated with red dashed lines. In order to validate the numerical predictions, the experimental characterization data reported by Smith in reference [55] for the same composite material investigated herein are included in the figure. It can be seen that the 3D model fits the data slightly better, especially in the high volume fraction region. Interestingly, it is noted that the uncertainty in the Young's modulus increases for larger filler contents (higher than 25%) in the 2D case, while the uncertainty in the elastic modulus when considering 3D RVEs remains almost constant. This fact evidences

the limitations related to the use of simplified 2D RVEs to reproduce the randomness in the three-dimensional distribution of particle-reinforced composites doped at moderate to high filler volume fractions.

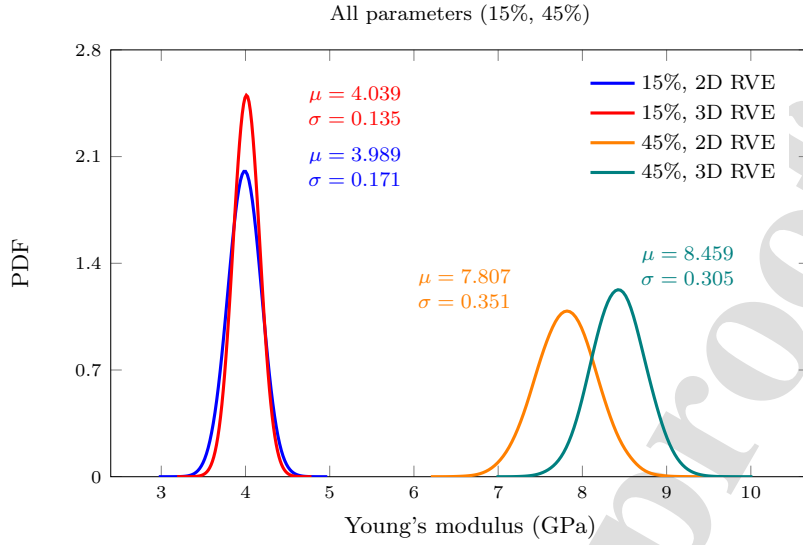


Figure 14: PDFs of the Young's modulus of epoxy doped with 15% and 45% glass particles considering 2D (blue lines) and 3D (red lines) RVEs for simultaneous uncertainties in all the parameters.

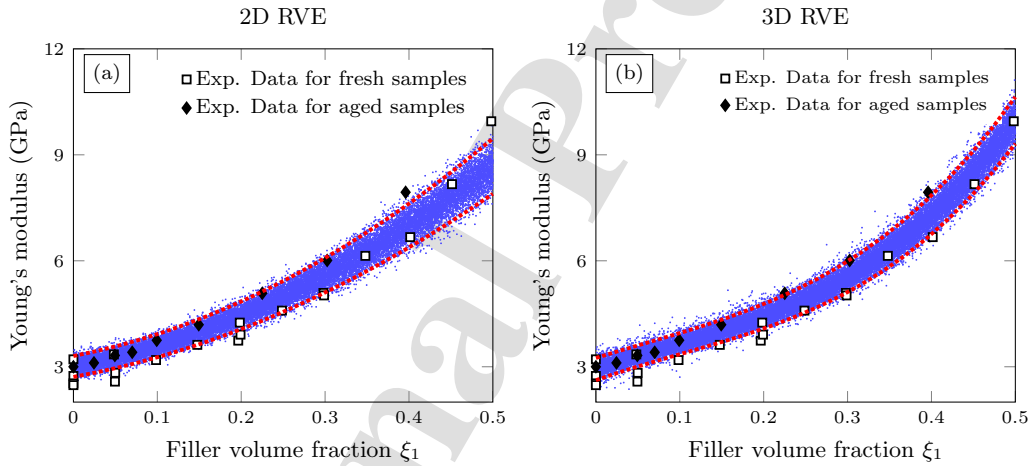


Figure 15: Comparison between the stochastic prediction of the Young's moduli of epoxy/glass fiber versus the filler volume fraction  $\xi_1$  in the 2D (a) and 3D (b) cases. The 95% confidence levels are indicated with red dashed lines. Experimental data retrieved from reference [55].

## 6. Conclusions

This work has investigated the surrogate modelling of 2D/3D highly computationally demanding numerical homogenisation problems of glass particles-reinforced epoxy composites. To this aim, PCE meta-modelling technique has been employed to bypass such computational intensive approaches and so perform uncertainty propagation analyses. Specifically, PCE-based uncertainty quantification analyses of the Young's modulus of epoxy/glass composites have been conducted for filler volume fractions up to 50%, using both 2D and 3D models. The statistical distributions of the micromechanical parameters of interest have been predefined, namely the filler volume

fraction, Young's modulus and the Poisson's ratio of the composite phases. Then, the design space has been sampled by means of Latin Hypercube Sampling in order to construct the PCE surrogate model. Finally, direct Monte Carlo simulations over the parameter space have been performed. The numerical results and discussion have proved the appropriateness of the developed schemes to conduct efficient uncertainty propagation analyses of the homogenisation parameters. The key conclusions of this research include:

- Optimal PCE surrogate models have been developed to approximate both 2D/3D homogenisation of epoxy composites doped with up to 50% volume fraction of glass filler particles using the dropping and rolling rules. Relationships between the minimal inter-particle distance and the filler volume fraction has been proposed for 2D and 3D RVEs, which represents a useful tool for the algorithm implementation.
- PCE meta-models have been defined through preliminary parametric analyses accounting for prediction accuracy and computational cost. To this aim, a set of local and global error metrics has been presented.
- The computing advantages of the developed meta-models have proved crucial to perform computationally intensive applications. Specifically, the presented results have showed their effectiveness to conduct fast uncertainty propagation analysis of epoxy composites doped with glass particles.
- The numerical results and discussion have evidenced the potential of the proposed approach for stochastic design and material selection applications. These open great opportunities for applications in material model design.
- For low and moderate filler volume fractions, it has been observed that both 2D and 3D models provide similar results, being the dispersion slightly higher when the 2D model is employed. On the other hand, for higher filler volume fractions, the discrepancies between the two models increase.
- In terms of sensitivity analysis, Sobol' indices of both models show that for a fixed volume fraction, uncertainties in the matrix properties dominate the uncertainty of the whole composite. Thus, following the above statement, for lower filler volume fractions, the material properties of the reinforcement can be set to their mean values and the homogenisation could be done using the 2D surrogate model without major changes in the final result.

The presented numerical results and discussion suggest the ability of the proposed methodology to be adapted to a large variety of composite materials. In this light, future developments regard the extension of the presented formulation to other composites with more complex microstructures, multi-physics homogenisation problems (e.g. piezoelectric materials), as well as the explicit modelling of the variability in the effective properties due to the randomness of the microstructure by developing a stochastic version of the presented surrogate model.

#### **Declaration of Competing Interest**

The authors declare that they have no known competing financial interests or personal relationships that could have appeared to influence the work reported in this paper.

## Acknowledgement

This work has been partially supported through Ministerio Ciencia e Innovación (Spain) [PID2020-116809GB-I00], by the Junta de Extremadura (Spain) through Research Group Grants [GR18023], and by the Ministerio de Economía y Competitividad (Spain) [DPI2017-89162-R], by the Consejería de Economía, Conocimiento, Empresas y Universidad de la Junta de Andalucía (Spain) [P18-RT-3128]. The last two projects were co-funded by the Fondo Europeo de Desarrollo Regional (FEDER), Programa Operativo FEDER 2014-2020.

## References

- [1] Oladele IO, Omotosho TF, Adediran AA. Polymer-Based Composites: An Indispensable Material for Present and Future Applications. *Int J Polym Sci* 2020.
- [2] Raju B, Hiremath SR, D Mahapatra DR. A review of micromechanics based models for effective elastic properties of reinforced polymer matrix composites. *Compos Struct* 2018; 204: 607-619.
- [3] Hill R. A self-consistent mechanics of composite materials. *J Mech Phys* 1965; 13 (4): 213–222.
- [4] Mori T, Tanaka K. Average stress in matrix and average elastic energy of materials with misfitting inclusions. *Acta metall* 1973; 21 (5): 571–574.
- [5] Guo Q, Yao W, Li W, Gupta, N. Constitutive models for the structural analysis of composite materials for the finite element analysis: A review of recent practices. *Compos Struct* 2020; 113267.
- [6] Hashin Z, Shtrikman S. A variational approach to the theory of the elastic behaviour of multiphase materials. *J Mech Phys Solids*, 1963; 11: 127–140.
- [7] Reuss A. Calculation of the flow limits of mixed crystals on the basis of the plasticity of mono-crystals. *Z Angew Math Mech* 1929; 9: 49–58.
- [8] Voigt W. Ueber die Beziehung zwischeden beiden Elasticitatsconstanten. *Ann Phys* 1889; 38: 573–587.
- [9] Clayton JD, Chung PW. An atomistic-to-continuum framework for nonlinear crystal mechanics based on asymptotic homogenization. *J Mech Phys Solids* 2006; 54 (8): 1604-1639.
- [10] Pace T, Rahmaninejad H, Sun B, Kekenus-Huskey P M. Homogenization of Continuum-Scale Transport Properties from Molecular Dynamics Simulations: An Application to Aqueous-Phase Methane Diffusion in Silicate Channels. *J Phys Chem B* 2021; 125(41): 11520–11533.
- [11] Artioli E, Beirão da Veiga L, Verani M. An adaptive curved virtual element method for the statistical homogenization of random fibre-reinforced composites. *Finite Elem Anal Des* 2020; 177: 103418.
- [12] Pingaro, M and Reccia, E and Trovalusci, P and Masiani, R. Fast statistical homogenization procedure (FSHP) for particle random composites using virtual element method. *Comput Mech* 2019; 64 (1): 197–210.
- [13] Marino, Michele and Hudobivnik, Blaž and Wriggers, Peter. Computational homogenization of polycrystalline materials with the Virtual Element Method. *Comput Methods Appl Mech Eng* 2019; 355:349–372.

- [14] To QD, Bonnet G. FFT based numerical homogenization method for porous conductive materials. *Comput Methods Appl Mech Eng* 2020; 368: 113160.
- [15] Ahmadi MH. A Stochastic Finite Element Analysis Framework for the Multiple Physical Modeling of Filler Modified Polymers PhD thesis University of Alberta, 2021
- [16] Reddy AC. Two dimensional (2D) RVE-Based Modeling of Interphase Separation and Particle Fracture in Graphite/5050 Particle Reinforced Composites. In 3rd National Conference on Materials and Manufacturing Processes, Hyderabad, India: 2002, 179–183.
- [17] Hill R. Elastic properties of reinforced solids: some theoretical principles. *J Mech Phys Solids* 1963; 11: 357-372.
- [18] Ostoja-Starzewski M. Material spatial randomness: From statistical to representative volume elemen. *Probabilistic Eng Mech* 2006; 21: 112-132.
- [19] García-Macías, Enrique and Ubertini, Filippo. Mathematical modeling and simulation. *Smart Nanoconcretes and Cement-Based Materials* 2020; 101–156.
- [20] Stroven M, Askes H, Sluys LJ. Numerical determination of representative volumes for granular materials. *Comput Mehtods Appl Engrg* 2004; 193: 3221-3238.
- [21] Naili, C and Doghri, I and Kanit, T and Sukiman, MS and Aissa-Berraies, A and Imad, A. Short fiber reinforced composites: Unbiased full-field evaluation of various homogenization methods in elasticity. *Compos Sci Technol* 2020; 187: 107942.
- [22] Teradaa K, Horib M, Kyoyac T, Kikuchid N. Simulation of the multi-scale convergence in computational homogenization approaches. *Int J Solids Struct* 2000; 37: 2285-2311.
- [23] Kanit T, Forest S, Galliet I, Mounoury V, Jeulin D. Determination of the size of the representative volume element for random composites: statistical and numerical approach. *Int J Solids Struct* 2003; 40: 3647-3679.
- [24] Gentieu T, Catapano A, Jumel J, Broughton J. Computational modelling of particulate-reinforced materials up to high volume fractions: Linear elastic homogenisation. *Proc Inst Mech Eng* 2019; 233 (6): 1101–1116.
- [25] Ma S, Zhuang X, Wang X. 3D micromechanical simulation of the mechanical behavior of an in-situ Al3Ti/A356 composite. *Compos B Eng* 2019; 176: 107115.
- [26] Nilenius F, Larsson F, Lundgren K, Runesson K. A 3d/2d comparison between heterogeneous mesoscale models of concrete. *Multi-Scale Modeling and Characterization of Infrastructure Material*. Dordrecht: Springer, 249-259, 2013.
- [27] Huang Y, Yan D, Yang Z, Liu G. 2D and 3D homogenization and fracture analysis of concrete based on in-situ X-ray Computed Tomography images and Monte Carlo simulations. *Eng Fract Mech* 2016; 163: 37-54.

- [28] Zeleniakienė D, Griškevičius P, Leišis V. The comparative analysis of 2D and 3D microstructural models stresses of porous polymer materials. *Mechanics* 2005; 53 (3): 22–26.
- [29] Kristiansen L, Alan Wouterse K, Philipse A. Simulation of random packing of binary sphere mixtures by mechanical contraction. *Phys A: Stat Mec. Appl* 2005; (2-4): 249–262.
- [30] Lubachevsky B D, Stillinger F H, Pinson E N. Disks vs. spheres: Contrasting properties of random packings. *J Stat Phys* 1991; 64 (3): 501–524.
- [31] Rintoul MD, Torquato S. Reconstruction of the structure of dispersions. *J Colloid Interface Sci* 1997; 186: 467–476.
- [32] Segurado J, Llorca J. A numerical approximation to the elastic properties of sphere-reinforced composites. *J Mech Phys* 2002; 50 (10): 2107–2121.
- [33] Shi Y, Zhang Y. Simulation of random packing of spherical particles with different size distributions. *Appl Phys A* 2008; 92 (3): 621–626.
- [34] Jodrey WS, Elmer MT. Simulation of random packing of spheres. *Simulation* 1979; 32(1): 1–12.
- [35] Cundall PA, Otto DLS. A discrete numerical model for granular assemblies. *Geotechnique* 1979; 29 (1): 47–65.
- [36] Thapa M, Mulani SB, Walters RW. Stochastic multi-scale modeling of carbon fiber reinforced composites with polynomial chaos. *Compos Struct* 2019; 213: 82–97.
- [37] Mohamedou M, Zulueta K, Chung CN, Rappel H, Beex L, Adam L, Noels L. Bayesian identification of mean-field homogenisation model parameters and uncertain matrix behavior in non-aligned short fiber composites. *Comp Struct* 2019; 220: 64-80.
- [38] Dey S, Mukhopadhyay T, Khodaparast HH, Adhikari S. Fuzzy uncertainty propagation in composites using Gram–Schmidt polynomial chaos expansion. *Appl Math Model* 2016; 407 (8): 4412–4428.
- [39] Peng X, Li D, Wu H, Liu Z, Li J, Jiang S, Tan J. Uncertainty analysis of composite laminated plate with data-driven polynomial chaos expansion method under insufficient input data of uncertain parameters. *Comp Struct* 2019; 209: 625–633.
- [40] Østergård T, Jensen RL, Maagaard SE. A comparison of six metamodeling techniques applied to building performance simulations. *Appl Energy* 2018; 211: 89–103.
- [41] Sun X, Choi YY, Choi JI. Global sensitivity analysis for multivariate outputs using polynomial chaos based surrogate models. *Appl Math Model* 2020; 82: 867–887.
- [42] Xiu D, Karniadakis GE. Modeling uncertainty in flow simulations via generalized polynomial chaos. *J Compu Phys* 2003; 1871: 137–167.
- [43] Smith RC. *Uncertainty Quantification*, 1st edn. SIAM, Philadelphia, 2014.

- [44] B. Efron B, Hastie T, Johnstone I, Tibshirani R. Least angle regression. *Ann Stat* 2004; 32 (2): 407–499.
- [45] Henyš, Petr and Čapek, Lukáš and Březina, Jan. Comparison of current methods for implementing periodic boundary conditions in multi-scale homogenisation. *Eur J Mech A Solids* 2019; 78: 103825.
- [46] Zhou J, Zhang Y, Chen JK. Numerical simulation of random packing of spherical particles for powder-based additive manufacturing. *J Manuf Sci Eng Trans ASME* 2009; 131 (3): 031004
- [47] Berger H, Kari S, Gabbert U, Rodríguez-Ramos R, Bravo-Castillero J, Guinovart-Díaz RA. Comprehensive numerical homogenisation technique for calculating effective coefficients of uniaxial piezoelectric fibre composites. *Mater Sci Eng A* 2005; 412 (1-2): 53–60.
- [48] Sudret B. Polynomial chaos expansions and stochastic finite element methods. *Risk Reliab Geotech Eng* 2014; 624: 265–300.
- [49] Blatman G, Sudret B. Adaptive sparse polynomial chaos expansion based on least angle regression. *J Comput Phys* 2011; 230: 2345–2367.
- [50] MATLAB and Statistics Toolbox Release 2012b, The MathWorks, Inc., Natick, Massachusetts, United States.
- [51] Ansys® Academic Research Mechanical, Release 18.1, Help System, Mechanical APDL Guide, ANSYS, Inc.
- [52] Ju J, Yanase K. Micromechanics and effective elastic moduli of particle-reinforced composites with near-field particle interactions. *Acta Mech* 2010; 215 (1) 135–153.
- [53] Schjødt-Thomsen J, Ryszard P. The Mori–Tanaka stiffness tensor: diagonal symmetry, complex fibre orientations and non-dilute volume fractions. *Mech Mater* 2001; 33 (10): 531-544.
- [54] McKay MD, Beckman RJ, Conover WJ. A comparison of three methods for selecting values of input variables in the analysis of output from a computer code. *Technometrics* 2000; 42 (1): 55–61.
- [55] Smith JC. Experimental values for the elastic constants of a particulate-filled glassy polymer. *J. Res. Natl. Bur. Stand. (U. S.)* 1976; 80 (1), 45-49.

**Declaration of Competing Interest**

The authors declare that they have no known competing financial interests or personal relationships that could have appeared to influence the work reported in this paper.



D. José Carlos García-Merino

Journal Pre-proof